JOURNAL OF MODERN OPTICS, 2002, VOL. 49, NO. 3/4, 335–347

Atomic coherence induced Kerr nonlinearity enhancement in Rb vapour

HAI WANG† D. J. GOORSKEY and MIN XIAO*

Department of Physics, University of Arkansas, Fayetteville, Arkansas 72701, USA

(*Received 15 March 2001; revision received 27 May 2001*)

Abstract. The Kerr nonlinear index of refraction for rubidium atoms is measured by using an optical ring cavity with and without electromagnetically induced transparency (EIT). Significant enhancement and inhibition of the Kerr nonlinear index is observed near resonance with EIT. The nonlinear index of refraction is measured as functions of probe and coupling frequency detunings, respectively, with and without the presence of EIT. A simple theoretical calculation including Doppler broadening is presented and is found to be in good qualitative agreement with the experimentally measured results.

1. Introduction

Multi-level atomic systems with electromagnetically induced transparency (EIT) [1–4] have been shown to enhance nonlinear optical processes such as frequency conversion [5–8] and four-wave mixing [9–11]. Enhanced third-order Kerr-type nonlinearity $\chi^{(3)}$ generated in multi-level atomic systems due to atomic coherence together with reduced absorption is responsible for such efficient nonlinear optical processes. Such enhanced Kerr nonlinearity also has various useful applications such as in cross-phase modulation for optical shutters [13] and self-phase modulation for generation of optical solitons [14]. In recent years, EIT and enhancement of linear and nonlinear susceptibilities with reduced absorption in multi-level atomic systems have attracted much interest [1–23]. Large nonlinear susceptibilities at low light powers are desirable for realization of photon blockades and single-photon nonlinear devices [13, 20–22]. To understand and optimize these nonlinear optical processes, one needs to have precise knowledge of the Kerr nonlinear coefficient n_2 as functions of other parameters such as pumping power and frequency detuning. Although many papers have been published on enhancing nonlinear optical processes, no direct experimental measurements of $\chi^{(3)}$ or n_2 have been reported, so far, in such multi-level atomic systems with atomic coherence conditions satisfied.

This paper presents experimental results in measuring the nonlinear Kerr index of refraction for three-level rubidium atoms inside an optical ring cavity with

† Permanent address: Institute of Optoelectronics, Shanxi University, Taiyuan 030006, People's Republic of China.

* Author for correspondence: e-mail: mxiao@mail.uark.edu

Journal of Modern Optics ISSN 0950–0340 print/ISSN 1362–3044 online
http://www.tandf.co.uk/journals
DOI: 10.1080/09500340110089938

and without EIT. Significant enhancement of the Kerr nonlinear coefficient is found in certain frequency ranges near resonance. Section 2, presents a simple theoretical treatment of the nonlinear index of refraction for a three-level atomic system including the Doppler effect. Section 3 describes the principle behind the cavity-scanning method used to measure n_2. Section 4 follows with a description of the experimental set-up and procedure, after which experimental results are discussed and compared with a theoretical model in Section 5. Section 6 gives a brief conclusion.

2. Theoretical model

In this section, a simple theoretical calculation is presented of the nonlinear susceptibility from density-matrix equations for three-level atoms, keeping the lowest nonlinear term for the probe field. A three-level Λ-type system in the D_1 lines of ^{87}Rb is considered, as shown in figure 1. A strong coupling laser of frequency ω_c near the ω_{23} resonance couples levels $|2\rangle$ and $|3\rangle$, while a weaker probe beam with frequency ω_p near the ω_{21} resonance couples levels $|2\rangle$ and $|1\rangle$. For this system the following equations are derived for the slowly varying density matrix elements [2, 24]:

$$\begin{aligned}
\dot{\rho}_{11} &= \gamma_{31}(\rho_{33} - \rho_{11}) + \gamma_{21}\rho_{22} - \frac{\mathrm{i}}{2}\Omega_p^*\rho_{21} + \frac{\mathrm{i}}{2}\Omega_p\rho_{21}^*, \\
\dot{\rho}_{22} &= -(\gamma_{23} + \gamma_{21})\rho_{22} - \frac{\mathrm{i}}{2}\Omega_p\rho_{21}^* + \frac{\mathrm{i}}{2}\Omega_p^*\rho_{21} - \frac{\mathrm{i}}{2}\Omega_c\rho_{23}^* + \frac{\mathrm{i}}{2}\Omega_c^*\rho_{23}, \\
\dot{\rho}_{33} &= \gamma_{31}(\rho_{11} - \rho_{33}) + \gamma_{23}\rho_{22} - \frac{\mathrm{i}}{2}\Omega_c^*\rho_{23} + \frac{\mathrm{i}}{2}\Omega_c\rho_{23}^*, \\
\dot{\rho}_{21} &= -(\gamma - i\Delta_p)\rho_{21} + \frac{\mathrm{i}}{2}\Omega_p(\rho_{22} - \rho_{11}) - \frac{\mathrm{i}}{2}\Omega_c\rho_{31}, \\
\dot{\rho}_{23} &= -(\gamma - i\Delta_c)\rho_{23} + \frac{\mathrm{i}}{2}\Omega_c(\rho_{22} - \rho_{33}) - \frac{\mathrm{i}}{2}\Omega_p\rho_{31}^*, \\
\dot{\rho}_{31} &= -[\gamma_{31} - i(\Delta_p - \Delta_c)]\rho_{31} + \frac{\mathrm{i}}{2}\Omega_p\rho_{23}^* - \frac{\mathrm{i}}{2}\Omega_c^*\rho_{21},
\end{aligned} \tag{1}$$

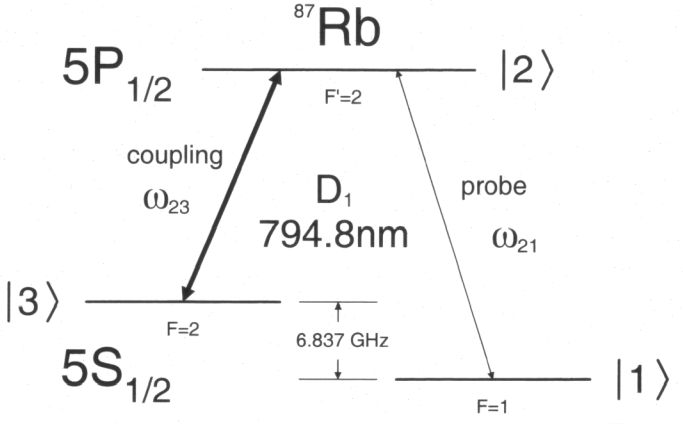

Figure 1. Three-level Λ-type system in the D_1 line of ^{87}Rb.

where $\Omega_p = -\mu_{12}E_p/\hbar$ and $\Omega_c = -\mu_{32}E_c/\hbar$ are the complex Rabi frequencies associated with the probe and coupling beams, respectively; $\Delta_p = \omega_p - \omega_{21}$ and $\Delta_c = \omega_c - \omega_{23}$ are the probe and coupling detunings, respectively; and $\gamma \equiv (\gamma_{21} + \gamma_{23} + \gamma_{31})/2$. The nonradiative decay between the levels $|3\rangle$ and $|1\rangle$ is expressed by γ_{31}, the decay rate from $|2\rangle$ to $|1\rangle$ is given by γ_{21}, and the decay rate from $|2\rangle$ to $|3\rangle$ is given by γ_{23}. The laser linewidths, $\delta\omega_p$ and $\delta\omega_c$, can be taken into account by including them in the decay rates as: $\gamma \longrightarrow \gamma + \delta\omega_p$, $\gamma_{31} \longrightarrow \gamma_{31} + \delta\omega_p + \delta\omega_c$ [2].

In order to derive the equations for the linear and nonlinear susceptibilities, we need to solve the density matrix equations (1) at steady state. An iterative technique is used to achieve increasingly accurate approximations to the matrix elements. The density matrix elements can be written as $\rho_{mn} = \rho_{mn}^{(0)} + \rho_{mn}^{(1)} + \rho_{mn}^{(2)} + \rho_{mn}^{(3)} + \cdots$, where each successive approximation is calculated using the matrix elements of one order less than the one being calculated. Several important assumptions are made. Under the condition that the coupling field is much stronger than the probe field, it can be assumed that all the atoms are (to zeroeth order) in the ground state $|1\rangle$, i.e. $\rho_{11}^{(0)} \approx 1$, $\rho_{22}^{(0)} \approx 0$, and $\rho_{33}^{(0)} \approx 0$. Under the weak-probe approximation, an expression can be obtained for ρ_{21} and ρ_{23} in the first order as:

$$\rho_{21}^{(1)} \approx \frac{\frac{\mathrm{i}}{2}\Omega_p(\rho_{22}^{(0)} - \rho_{11}^{(0)})}{\gamma - i\Delta_p + \dfrac{|\Omega_c|^2/4}{\gamma_{31} - \mathrm{i}(\Delta_p - \Delta_c)}} \approx \frac{-\frac{i}{2}\Omega_p}{\gamma - i\Delta_p + \dfrac{|\Omega_c|^2/4}{\gamma_{31} - i(\Delta_p - \Delta_c)}}, \tag{2}$$

and

$$\rho_{23}^{(1)} \approx 0.$$

To obtain the third order in ρ_{21} we need to know $\rho_{22} - \rho_{11}$ to the second order, which is

$$\rho_{22}^{(2)} - \rho_{11}^{(2)} \approx \frac{2}{2\gamma + \gamma_{21}}\left[\mathrm{i}\Omega_p^*\rho_{21}^{(1)} - \mathrm{i}\Omega_p\rho_{21}^{(1)*}\right] + \frac{2}{2\gamma + \gamma_{21}}. \tag{3}$$

Here, $\rho_{33}^{(2)}$ can be neglected. With the above procedure, ρ_{21} is calculated up to third order as:

$$\rho_{21} \approx \rho_{21}^{(1)} + \rho_{21}^{(3)} \approx -\frac{\mathrm{i}\Omega_p}{2F}\left(1 - \frac{2\gamma_{31}}{2\gamma + \gamma_{21}}\right) + \frac{\mathrm{i}\Omega_p}{2F}\frac{|\Omega_p|^2}{2\gamma + \gamma_{21}}\left(\frac{1}{F} + \frac{1}{F^*}\right), \tag{4}$$

where

$$F \equiv \gamma - \mathrm{i}\Delta_p + \frac{|\Omega_c|^2/4}{\gamma_{31} - \mathrm{i}(\Delta_p - \Delta_c)}. \tag{5}$$

The total polarization $\vec{P}(t)$ of the atomic medium can be expressed simply as linear polarized light for the proposed experimental arrangement and is given by

$$\mathrm{P} = N\left[\rho_{21}d_{12}\mathrm{e}^{-\mathrm{i}\omega_p t} + \rho_{21}^* d_{12}^* \mathrm{e}^{\mathrm{i}\omega_p t}\right]. \tag{6}$$

Since the polarization can also be written as

$$\mathrm{P} = \frac{1}{2}\epsilon_0\left[E_p\chi\mathrm{e}^{-\mathrm{i}\omega_p t} + E_p^*\chi^*\mathrm{e}^{\mathrm{i}\omega_p t}\right], \tag{7}$$

where χ is the susceptibility of the atomic medium, by comparing equations (6) and (7) it can be concluded that

$$\chi = \frac{2Nd_{12}}{\epsilon_0 E_p}\rho_{21}. \tag{8}$$

From equation (4), expressions can be obtained for the first-order and third-order susceptibilities as

$$\chi^{(1)} = \frac{\mathrm{i}N|d_{21}|^2}{\epsilon_0\hbar}\frac{1}{F}\left(1 - \frac{2\gamma_{31}}{2\gamma + \gamma_{21}}\right), \tag{9}$$

and

$$\chi^{(3)} = -\frac{\mathrm{i}N|d_{21}|^4}{3\epsilon_0\hbar^3}\frac{1}{(2\gamma + \gamma_{21})}\frac{1}{F}\left[\frac{1}{F} + \frac{1}{F^*}\right], \tag{10}$$

where $\chi = \chi^{(1)} + 3|E_p|^2\chi^{(3)}$ and d_{21} is the dipole moment for the $|2\rangle \longrightarrow |1\rangle$ transition.

An atomic vapour cell is considered here to match the experimental situation. Although the first-order Doppler effect can be eliminated by the two-photon Doppler-free configuration (i.e. co-propagating in the Λ-type system), the residual Doppler effect due to the energy difference between probe and coupling transitions needs to be taken into account by the following integration over the atomic velocity distribution [2]. If an atom is moving with velocity v against the propagation direction of the probe beam, it will see the probe beam's frequency up-shifted to $\omega_p + (v/c)\omega_p$. Similarly, since the coupling beam is co-propagating with the probe beam, the same atom will see the coupling beam's frequency to be up-shifted to $\omega_c + (v/c)\omega_c$. This causes an increase in the detunings: $\Delta_p' = \Delta_p + (v/c)\omega_p$ and $\Delta_c' = \Delta_c + (v/c)\omega_c$. It can be assumed that the components of the atomic velocities which lie along the beam axis obey a Maxwellian distribution:

$$\mathrm{d}N(v) = \frac{N_0}{u\sqrt{\pi}}\mathrm{e}^{-v^2/u^2}\mathrm{d}v, \tag{11}$$

where $u/\sqrt{2}$ is the root mean square atomic velocity and N_0 is the total atomic density of the vapour. In this way the Doppler effect can be included in the susceptibilities as:

$$\chi^{(1)}(v)\mathrm{d}v = \frac{\mathrm{i}|d_{21}|^2}{\epsilon_0\hbar}\frac{1}{F(v)}\left(1 - \frac{2\gamma_{31}}{2\gamma + \gamma_{21}}\right)\mathrm{d}N(v), \tag{12}$$

and

$$\chi^{(3)}(v)\mathrm{d}v = -\frac{\mathrm{i}|d_{21}|^4}{3\epsilon_0\hbar^3}\frac{1}{(2\gamma + \gamma_{21})}\frac{1}{F(v)}\left[\frac{1}{F(v)} + \frac{1}{F^*(v)}\right]\mathrm{d}N(v), \tag{13}$$

where F has changed to

$$F(v) = \gamma - \mathrm{i}\left(\Delta_p + \frac{v}{c}\omega_p\right) + \frac{|\Omega_c|^2/4}{\gamma_{31} - \mathrm{i}(\Delta_p - \Delta_c) - \mathrm{i}\dfrac{v}{c}(\omega_p - \omega_c)}. \tag{14}$$

To get total susceptibility, it is necessary to integrate over the velocity v from $-\infty$ to $+\infty$, as

$$\chi = \int_{-\infty}^{+\infty} \chi(v)\, \mathrm{d}v. \tag{15}$$

The numerical results of this integrated susceptibility will be given as functions of Δ_p and Δ_c in section 5 in comparison with experimentally measured results.

3. Nonlinear phase shift of a medium inside an optical ring cavity

In our experiment, an optical ring cavity is used to measure the nonlinear Kerr index of refraction n_2. This technique was used previously to measure the nonlinear phase shift in the intracavity second harmonic generation process [25]. The condition for cavity resonance is that the total round-trip phase Φ^{TOT} needs to be an integer multiple of 2π. The phase shift of the cavity field travelling through the vapour cell is related to the index of refraction of the atomic medium. This index of refraction to a probe beam of intensity I_p can be written as $n = n_0 + n_2 I_p$, where n_0 is the linear index of refraction and n_2 is the nonlinear Kerr index of refraction. These indexes of refraction are related to the first-order and third-order susceptibilities, $\chi^{(1)}$ and $\chi^{(3)}$, according to the relations (in Gaussian units) [26]:

$$n_0 = \sqrt{1 + 4\pi\ \mathrm{Re}\chi^{(1)}}, \tag{16}$$

$$n_2 = \frac{12\pi^2}{n_0^2 c}\mathrm{Re}\chi^{(3)}. \tag{17}$$

By keeping the frequencies of the probe and coupling lasers constant, we scan the cavity length linearly with time. As the cavity length approaches the resonant length of the cavity, the intracavity intensity of the probe beam builds up. Owing to the nonlinear Kerr effect, the index of refraction changes which results in a change in the phase detuning condition defined as $\delta = \Phi^{TOT} - 2\pi m$ for integer m. If $n_2 < 0$, then as the cavity length approaches the cavity resonant length from below, the build-up of the circulating intensity causes an effective increase in the cavity resonant length through the nonlinear phase. Thus, the cavity resonance will not be reached as fast, compared with the linear case. As the cavity length is scanned further, the drop-off of the cavity transmission will be steeper than in the linear case. As a result, if the cavity output is detected by a detector and displayed on an oscilloscope as intensity versus time, the cavity output transmission peak will be asymmetric with respect to time, as shown in figure 2. In the linear case (for very low probe intensity), the cavity transmission shows only a symmetric temporal profile.

We can take advantage of this effect to measure the nonlinear Kerr index of refraction n_2 directly without worrying about the linear contributions to the susceptibility. For an optical ring cavity [25],

$$\delta = \frac{\omega_p L}{c} + \frac{(n_0 - 1)\omega_p \ell}{c} + \frac{\omega_p \ell}{c} n_2 I_p - 2\pi m, \tag{18}$$

where ω_p is the probe frequency, L is the cavity length, and ℓ is the length of the vapour cell. When the cavity length is scanned linearly with time, the phase detuning can be expressed as

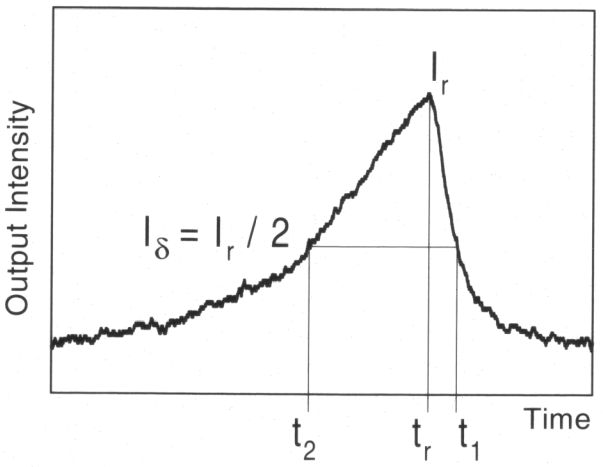

Figure 2. An asymmetric cavity transmission profile with nonlinear phase shift. Definitions of the parameters t_1, t_2, t_r, I_r, and I_δ are shown.

$$\delta = A(t - t_0) + \frac{\omega_p \ell}{c} n_2 I_p, \tag{19}$$

where t_0 is the time when $\delta = 0$ in the linear case. The constant A can be obtained by measuring the time between two adjacent resonant peaks τ and is given by $A = 2\pi/\tau$. We define the degree of asymmetry Δ to be

$$\Delta = (t_1 - t_r) - (t_r - t_2), \tag{20}$$

where t_r is the time at which the output intensity is peaked, t_1 and t_2 are the times on either side of the resonant peak at which the output intensity is some particular fraction (1/2 for simplicity) of the maximum intensity at resonance, as shown in figure 2. The nonlinear Kerr index of refraction is then given as

$$n_2 = \frac{c}{2\omega_p \ell} \frac{A\,\Delta}{(I_r - I_\delta)}, \tag{21}$$

where $I_\delta = I_r/2$ is the intensity at times t_1 and t_2. In this way we can obtain n_2 simply by measuring the degree of asymmetry in the transmission peak's temporal profile.

4. Experimental arrangement

The experimental set-up is shown in figure 3 and is very similar to an earlier experiment measuring cavity linewidth narrowing with an EIT system [27]. The coupling laser (LD1) and probe laser (LD2) are single-mode tunable Hitachi HL7851G diode lasers which are current and temperature stabilized. A feedback control loop further stabilizes each laser. The probe laser and coupling laser linewidths ($\delta\omega_p$ and $\delta\omega_c$) are both about $2\pi\times0.5$ MHz. A small amount (about 10%) of the probe and coupling beams are separated out from the laser beams using two polarizing beamsplitters (PBS1 and PBS2) and directed into a saturation absorption spectrometer (SAS). The output of the SAS is received by a detector (D3).

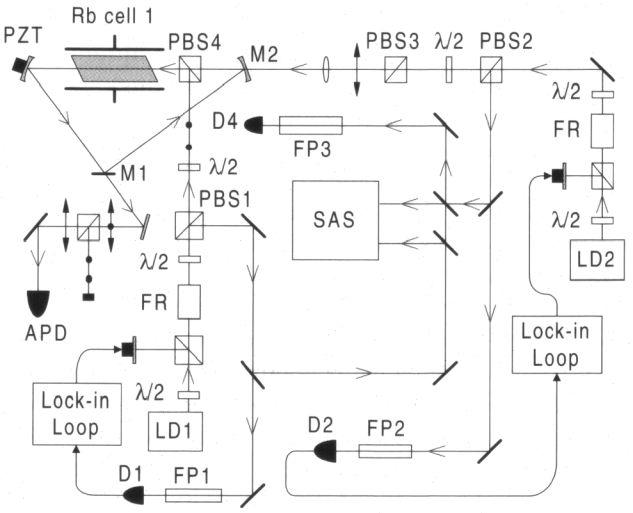

Figure 3. The experimental set-up: LD1 and LD2, coupling and probe lasers, respectively; PBS1–PBS5, polarizing cubic beam splitters; $\lambda/2$, half-wave plates; FR, Faraday Rotators; FP1–FP3, Fabry–Perot cavities; D1–D4 detectors; APD, avalanche photodiode detector. Other abbreviations are defined in the text.

This is used for monitoring the coupling and probe detunings (Δ_c and Δ_p) from their respective atomic transitions (ω_{23} and ω_{21}).

In this experiment the Kerr nonlinear index of refraction n_2 is measured as a function of probe and coupling detunings (Δ_p and Δ_c) independently with EIT and without EIT. In order to measure the detuning, either Δ_p or Δ_c, a confocal Fabry-Perot cavity (FP3) is used.

The optical ring cavity is formed using three mirrors. The flat mirror (M1) and concave mirror (M2, R = 10 cm) have about 1% and 3% transmissivities, respectively. The third mirror (PZT, concave, with R = 10 cm) is mounted on a PZT and has a reflectivity greater than 99.5%. The finesse of the empty cavity is about 100 with a free spectral range of 822 MHz (cavity length = 37 cm). The rubidium vapour cell (Rb cell 1) is 5 cm long with Brewster angle windows to eliminate back reflections. The cell is wrapped in μ-metal for magnetic field shielding and heat tape for temperature control. The probe beam enters the cavity through mirror (M2) and the coupling beam is brought into the cavity through PBS4. The coupling and probe beams co-propagate through the Rb vapour cell and are orthogonally polarized. The coupling beam is aligned at a 2° angle to the probe beam and they intersect in the centre of the Rb cell. This misalignment is enough to keep the coupling beam from circulating in the cavity. The probe beam is focused to the centre of the Rb cell using a 15 cm focal length lens. The radii of the coupling and probe beams are estimated to be 700 μm and 80 μm, respectively. Owing to losses from PBS4 and the Rb vapour cell, the Finesse (to the probe beam with frequency far from the atomic transition frequency ω_{21}) is reduced to about 50. The input intensity of the probe beam is controlled by PBS3 and a half-wave plate ($\lambda/2$).

The power of the coupling beam entering the Rb cell is kept constant at about 20mW and is estimated to have a Rabi frequency of $\Omega_c = 2\pi \times 72$ MHz at the centre

of the Rb cell. The intracavity intensity of the probe beam varies as the cavity length is scanned across the cavity resonance. The maximum intracavity intensity is highly dependent on the probe and coupling detunings, Δ_p and Δ_c, due to the EIT absorption profile. In order to achieve consistency in measurements of n_2 throughout the whole range of frequency detunings, the peak intracavity probe power is kept at near 6 μW for each measurement. This is easily done by adjusting the probe's input power to take advantage of saturation of absorption in the $|1\rangle \longrightarrow |2\rangle$ transition. The peak Rabi frequency of the probe beam at the centre of the Rb cell is then estimated to be $\Omega_p = 2\pi \times 11$ MHz.

The EIT profile without optical cavity has been reported previously [3]. Under the current experimental conditions, the resonant absorption is still 45% and the width of the EIT transmission spike is about 19 MHz.

The probe and coupling lasers are frequency-locked, so in order to observe the cavity transmission, the length of the cavity is scanned through resonance. The probe and coupling beams are separated at the cavity output by using another polarizing beam splitter. The output from the cavity is picked up by an avalanche photodiode (APD).

5. Results and discussion

First, the coupling detuning (Δ_c) is set to zero and the probe detuning Δ_p is tuned to different values. The temporal transmission profile of the cavity output with a small probe detuning (a few MHz) is observed to be highly asymmetric with the presence of EIT [28]. Figure 4 shows the cavity transmission profiles for two different probe detunings ($\Delta_p = \pm 7$ MHz) with and without EIT. Without the coupling beam, the transmission profile is nearly symmetric in time. When the

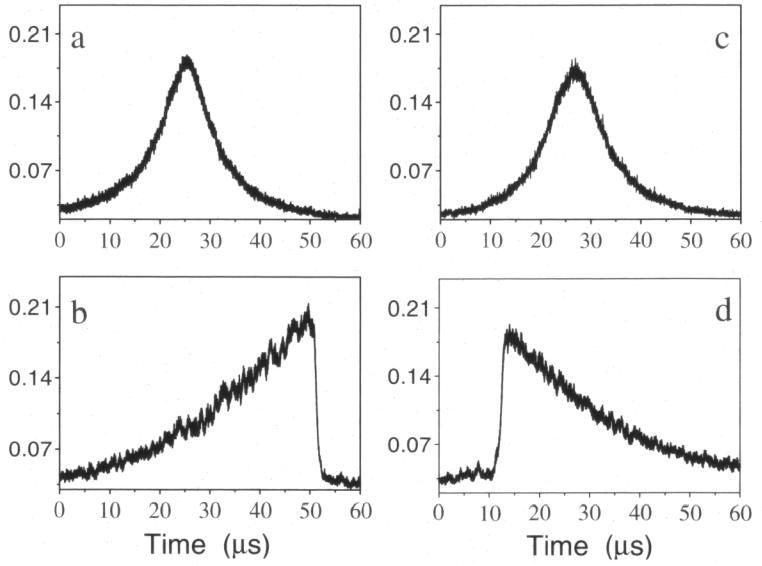

Figure 4. Cavity transmission profiles for $\Delta_c = 0$. (*a*) No EIT and $\Delta_p = +7$ MHz. (*b*) With EIT and $\Delta_p = +7$ MHz. (*c*) No EIT and $\Delta_p = -7$ MHz. (*d*) With EIT and $\Delta_p = -7$ MHz.

coupling beam is turned on and the probe detuning is set at $\Delta_p = +7$ MHz, the cavity output increases slowly to the maximum at resonance and subsequently undergoes a sharp drop-off as the cavity length is increased further, as shown in figure 4(*b*), corresponding to a negative nonlinear index of refraction ($n_2 < 0$). As the cavity length gets near the resonant cavity length, the circulating intensity of the probe beam builds up. With an increase in intensity, for a negative n_2, the phase detuning δ, as given in equation (18), will be hindered from approaching zero. The opposite happens when the cavity length is increased beyond the cavity resonance and the sharp drop-off in the cavity output intensity is observed. When the probe detuning is set to $\Delta_p = -7$ MHz, the cavity transmission has a reversed profile, as shown in figure 4(*d*), indicating a positive nonlinear index of refraction ($n_2 > 0$). The values of the nonlinear Kerr index of refraction for zero coupling detuning ($\Delta_c = 0$) and probe detunings of $+7$ MHz and -7 MHz with EIT were measured to be about $-6.2\times10^{-6}\text{cm}^2\text{W}^{-1}$ and $7.1\times10^{-6}\text{cm}^2\text{W}^{-1}$, respectively.

The nonlinear Kerr index of refraction was measured as a function of probe detuning with and without EIT for $\Delta_c = 0$. The results are plotted in figure 5. The solid squares are the values of n_2 that were measured with EIT while the open circles were measured without EIT. From this figure one can easily see the significant differences that atomic coherence makes in the nonlinear index of refraction. In addition to the large increase in the nonlinear index, the presence of an EIT dip causes the nonlinear index to be zero at two additional points besides the $\Delta_p = 0$ point. Furthermore, the sign and slope of n_2 as a function of probe detuning are opposite to that of the linear index of refraction n_0, as can be easily seen from equations (12)–(14) together with equations (16) and (17). The presence of EIT enhances the nonlinear Kerr effect by more than a factor of 100 for certain probe detunings ($\Delta_p = \pm7$ MHz) in our experiment. With improvements in laser linewidths, elimination of cavity losses, and reduction of atomic transient effects in the cell, one can expect to increase the Kerr nonlinear coefficient to a much higher value. The increase in n_2 for $\Delta_p > 200$ MHz is mainly due to the optical pumping effect.

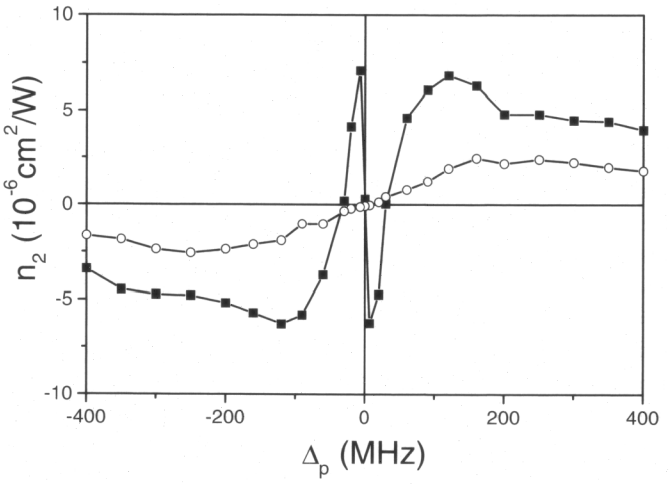

Figure 5. Experimental nonlinear index of refraction n_2 versus probe detuning Δ_p for $\Delta_c = 0$. ■ are data points with EIT and ○ are data points without EIT.

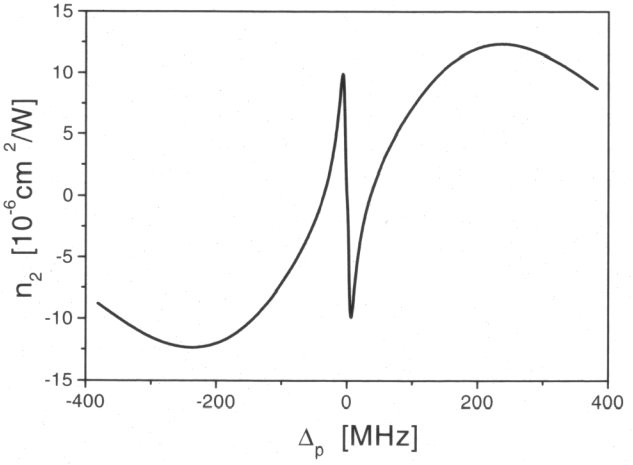

Figure 6. Theoretical plot of nonlinear index of refraction n_2 versus probe detuning Δ_p for $\Delta_c = 0$ with EIT. ($\gamma_{21} = 2\pi \times 3.0$ MHz, $\gamma_{31} = 2\pi \times 1.1$ MHz, $\gamma = 2\pi \times 3.5$ MHz, $\Omega_c = 2\pi \times 72$ MHz, $d_{21} = 4.45 \times 10^{-18}$ e.s.u., $N_0 = 4.5 \times 10^{11}$ atoms cm^{-3} at $T = 63°$C).

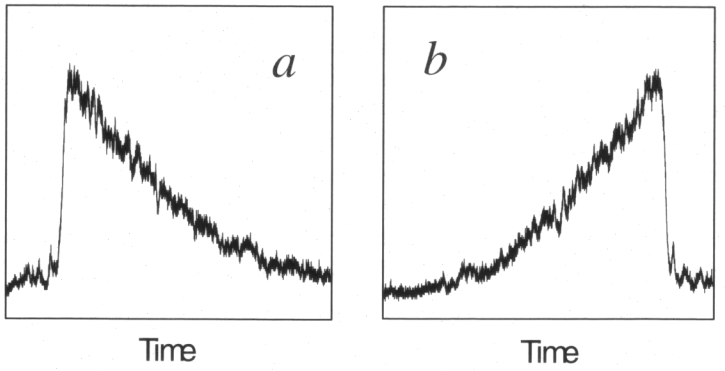

Figure 7. Cavity transmission profiles for $\Delta_p = 0$ with EIT. (*a*) $\Delta_c = +7$ MHz. (*b*) $\Delta_c = -7$ MHz.

Figure 6 plots a graph of our theoretical calculation of the value of n_2 as a function of probe detuning with EIT and $\Delta_c = 0$, according to equation (13) with the Doppler effect included. This figure is in good agreement with the experimentally measured results shown in figure 5. By using experimental parameters, maximum calculated values of n_2 agree well with the measured values. However, owing to some simplifications made in the theoretical model, such as the plane-wave and mean field approximations in the cavity and the optical pumping effect, no attempt was made to make a quantitative match.

Next, the cavity transmission profile was measured for zero probe detuning ($\Delta_p = 0$) and small coupling detunings ($\Delta_c = \pm 7$ MHz) with EIT, as shown in figure 7. The behaviour of the cavity transmission profiles is similar to the cases when $\Delta_c = 0$ and Δ_p is offset by small values as shown in figures 4(*b*) and 4(*d*). The nonlinear Kerr index of refraction n_2 under these conditions was measured to be

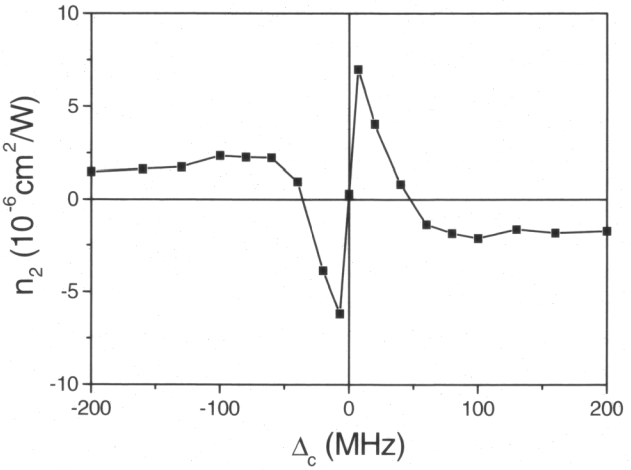

Figure 8. Experimental nonlinear index of refraction n_2 versus coupling detuning Δ_c for $\Delta_p = 0$ with EIT.

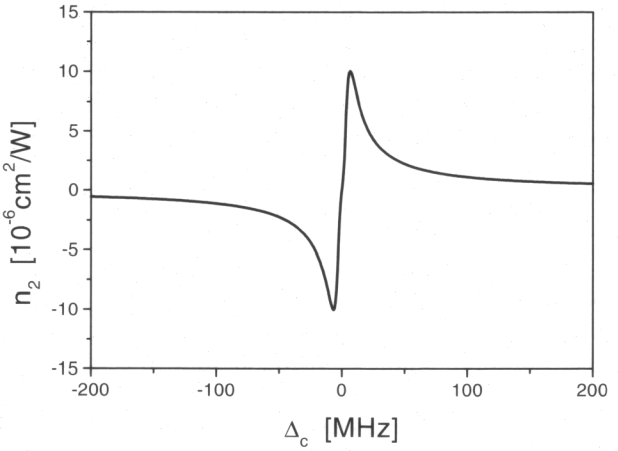

Figure 9. Theoretical plot of nonlinear index of refraction n_2 versus coupling detuning Δ_c for $\Delta_p = 0$ with EIT. ($\gamma_{21} = 2\pi \times 3.0$ MHz, $\gamma_{31} = 2\pi \times 1.1$ MHz, $\gamma = 2\pi \times 3.5$ MHz, $\Omega_c = 2\pi \times 72$ MHz, $d_{21} = 4.45 \times 10^{-18}$ e.s.u., $N_0 = 4.5 \times 10^{11}$ atoms cm^3 at $T = 63°$C).

about -7.0×10^{-6}cm^2 W^{-1} (for $\Delta_c = -7$ MHz) and 6.2×10^{-6}cm^2 W^{-1} (for $\Delta_c = +7$ MHz), respectively.

A graph of the nonlinear Kerr index of refraction versus coupling detuning with EIT and $\Delta_p = 0$ is shown in figure 8. The coupling frequency dependence of the nonlinear index n_2 is similar to the probe frequency dependence in that three zeros are present and the maximum values of n_2 are of the same order. However, the change of n_2 versus Δ_c is opposite in shape to the change of n_2 versus Δ_p which can be seen by examining equation (14). Theoretically calculations were made of the nonlinear index of refraction n_2 as a function of Δ_c for $\Delta_p = 0$ and the results are plotted in figure 9. One can see that the theoretical curve is in qualitative agreement with the experimentally measured results.

This research opens up the possibility of many new and interesting applications for nonlinear optical processes in multi-level atomic systems with EIT. For example, for zero probe detuning, as shown in figure 8, the nonlinear index is normal and approximately linear in the probe detuning range of ± 7 MHz, it should be possible to control self-focusing and other third-order nonlinear optical effects of the probe beam by changing the detuning of the coupling beam. With the measured Kerr nonlinear index of refraction under the EIT condition, one can optimize the nonlinear optical processes in such interesting systems. It will be interesting to study the large enhancement of the Kerr nonlinear coefficient in four-level systems at low light intensities [20–22].

We would like to point out that the nonlinear index of refraction n_2 measured in this experiment is different from that presented in [17]. In that work the nonlinear term is proportional to $n_2' I_c$ (inferred from the slope of the linear dispersion) which depends on the coupling intensity I_c (cross-phase modulation effect), while in our experiment the nonlinear term $n_2 I_p$ depends on the probe intensity (self-phase modulation effect). The self-phase nonlinearity in the index of refraction arises from the third-order nonlinear susceptibility $\chi^{(3)}$ for the probe beam while the cross-phase nonlinearity refers to the first-order susceptibility $\chi^{(1)}$ for the probe beam. This explains the difference in the n_2 values reported. Even when n_2 was measured as a function of coupling detuning and the probe detuning was fixed at zero, only the self-phase nonlinearity n_2 was measured, not the cross-phase nonlinearity n_2' as was done in [17]. Of course, n_2 is also a function of the coupling intensity as shown in equations (14) and (15).

6. Conclusion

In conclusion, we have directly measured the nonlinear Kerr index of refraction for multi-level rubidium atoms by using an optical ring cavity near resonance with and without EIT. The Kerr index was measured as functions of probe and coupling frequency detunings, respectively. It was found that the nonlinear Kerr index can both be enhanced and inhibited owing to the presence of EIT at different frequency detunings. The amplitude and sign of n_2 can be controlled simply by tuning the coupling frequency over a small frequency range (a few MHz). A simple theoretical treatment has been derived, based on a three-level Λ-type atomic system with higher order probe intensity, including Doppler broadening. It is found that the theoretical results are in good agreement with the experimental measurements. This work helps understanding of third-order nonlinear optical processes in such multi-level atomic systems involving atomic coherence and can lead to interesting applications in nonlinear optical devices such as all-optical switching.

Acknowledgments

We acknowledge funding support from the US National Science Foundation and the US Office of Naval Research.

References

[1] Boller, K. J., Imamoğlu, A., and Harris, S. E., 1991, *Phys Rev. Lett.*, **66,** 2595; Field, J. E., Hahn, K. H., and Harris, S. E., 1991, *Phys. Rev. Lett.*, **67,** 3062.

[2] Gea-Banacloche, J., Li, Y., Jin, S., and Xiao, M., 1995, *Phys Rev.* A, **51,** 576.

[3] Li, Y., and Xiao, M., 1995, *Phys Rev. A: Rapid Commun.*, **51,** R2703.

[4] Harris, S. E., 1997, *Phys. Today*, **50**(7), 36.

[5] Hakuta, K., Marmet, L., Stoicheff, B. P., 1991, *Phys. Rev. Lett.*, **66,** 596.

[6] Zhang, G. Z., Hakuta, K., and Stoicheff, B. P., 1993, *Phys. Rev. Lett.*, **71,** 3099.

[7] Jain, M., Xia, H., Yin, G. Y., Merriam, A. J., and Harris, S. E., 1996, *Phys. Rev. Lett.*, **77,** 4326.

[8] Hemmer, P. R., Kutz, D. P., Donoghue, J., Golomb, M., Sahriar, M. S., and Kumar, P., 1995, *Opt. Lett.*, **20,** 982.

[9] Marriam, A. J., Sharpe, S. J., Shverdin, M., Manuszah, D., Yin, G. Y., and Harris, S. E., 2000, *Phys. Rev. Lett.*, **84,** 5308.

[10] Li, Y., and Xiao, M., 1998, *Opt. Lett.*, **21,** 1064.

[11] Lü, B., Burkett, W. H., and Xiao, M., 1998, *Opt. Lett.*, **23,** 804.

[12] Kash, M. M., Sautenkov, V. A., Zibrov, A. S., Hollberg, L., Welch, G. R., Lukin, M. D., Rostovtsev, Y., Fry, E. S., and Scully, M. O., 1999, *Phys. Rev. Lett.*, **82,** 5229.

[13] Schmidt, H., and Imamoğlu, A., 1996, *Opt. Lett.*, **21,** 1936.

[14] Tikhonenko, V., Christou, J., and Luther-Davies, B., 1996, *Phys. Rev. Lett.*, **76,** 2698.

[15] Xiao, M., Li, Y., Jin, S., and Gea-Banacloche, J., 1995, *Phys. Rev. Lett.*, **74,** 666.

[16] Budker, D., Kimball, D. F., Rochester, S. M., and Yashchuk, V. V., 1999, *Phys. Rev. Lett.*, **83,** 1767.

[17] Hau, L. V., Harris, S. E., Dutton, Z., and Behroozi, C. H., 1999, *Nature*, **397,** 594.

[18] Phillips, D. F., Fleischhauer, A., Mair, A., Walsworth, R. L., and Lukin, M. D., 2001, *Phys. Rev. Lett.*, **86,** 783.

[19] Liu, C., Dutton, Z., Behroozi, C. H., and Hau, L. V., 2001, *Nature*, **401,** 490.

[20] Harris, S. H., and Yamamoto, Y., 1998, *Phys. Rev. Lett.*, **81,** 2611.

[21] Harris, S. E., and Hau, L. U., 1999, *Phys. Rev. Lett.*, **82,** 4601.

[22] Imamoğlu, A., Schmidt, H., Woods, G., and Deutsch, M., 1997, *Phys. Rev. Lett.*, **79,** 1467.

[23] Mulchan, N., Ducreay, D. G., Pina, R., Yan, M., and Zhu, Y., 2000, *J. Opt. Soc. Am.* B, **17,** 820.

[24] Scully, M. O., and Zubairy, M. S., 1997, *Quantum Optics* (Cambridge: Cambridge University Press).

[25] Ou, Z. Y., 1996, *Opt. Commun.*, **124,** 430.

[26] Boyd, R. W., 1992, *Nonlinear Optics* (New York: Academic Press).

[27] Wang, H., Goorskey, D. J., Burkett, W. H., and Xiao, M., 2000, *Opt. Lett.*, **25,** 1732.

[28] Wang, H., Goorskey, D. J., and Xiao, M., 2001, *Phys. Rev. Lett.*, **87,** 073601.